THE MEASUREMENT OF THE OUTPUT SPECTRUM OF A COBALT 60 TELETHERAPY UNIT

A

THESIS

Submitted to

THE FACULTY OF GRADUATE STUDIES

in Partial Fulfilment of

the Requirements for

THE DEGREE OF MASTER OF ARTS

in

THE DEPARTMENT OF PHYSICS

UNIVERSITY OF SASKATCHEWAN

by

JOHN WILLIAM SCRIMGER

Written Under the Supervision of Dr. D.V. CORMACK

Saskatoon, Saskatchewan

March, 1962

ACKNOWLEDGEMENTS

The author would like to express sincere thanks to Dr. D.V. Cormack for his advice and assistance throughout this project. The help of Mr. C. Kresse in the building and modification of equipment, and of Miss L. Schmidt in drafting, is gratefully acknowledged.

The facilities of the Co^{60} therapy room were placed at the author's disposal by kind permission of the Saskatoon Cancer Clinic.

Finally, the author wishes to express his appreciation to the National Cancer Institute for the financial assistance, given in the form of a fellowship, and in research grants.

ABSTRACT

The output spectrum of radiation emerging from a Co^{60} teletherapy unit contains a certain amount of low energy radiation in addition to the primary Co^{60} γ -rays with energies of 1.17 and 1.33 Mev. Since the beam strength is approximately 2×10^9 photons/cm^2/sec at 80 cm from the source, direct measurement of this spectrum was not practicable. The spectral distribution of single scattered radiation from this beam, at each of a number of scattering angles, was therefore measured. This scattered spectrum was then converted to the output spectrum by the application of the appropriate scattering equations.

The measured spectrum was corrected for crystal and photomultiplier tube distortions by means of a correction matrix. This matrix was formulated from information contained in a paper by Berger and Doggett on the response function of NaI(Tl) crystals, and was constructed such that its intervals were proportional to the square root of the photon energy. This provided more detail in the low energy region of the matrix.

The curves of the output spectrum obtained from various scattering angles were essentially the same, and the mean spectral curve compared favorably with the theoretical data derived by Cormack and Johns.

TABLE OF CONTENTS

LIST OF DIAGRAMS

LIST OF TABLES

TABLE OF CONTENTS

LIST OF DIAGRAMS

LIST OF TABLES

INTRODUCTION

When working with Co^{60} teletherapy units, it has been common practice to consider the γ-ray beam to consist of two energies of 1.17 and 1.33 Mev. For many purposes, however, this is an over-simplification, since there exists a measurable amount of low energy radiation in the output spectrum. This degraded energy arises principally from multiple Compton scattering within the Co source itself, and also scattering from the collimating system. Since a knowledge of the complete output spectrum is desirable, experiments to obtain this information are reported here.

The Co^{60} source at present housed in the teletherapy unit of the Saskatoon Cancer Clinic has an effective strength of about 1500 curies. Because of this high activity, and the resulting beam strength of 2×10^9 photons/cm^2/sec at 80 cm, it is extremely difficult to measure the output spectrum directly. Such a measurement would require that the beam be very highly collimated, and this would introduce considerable alignment difficulties. It would then be difficult to avoid spectral distortions. Another solution would be to separate the source and detector by a large distance, of the order of 10 metres or more, but physical limitations caused by the room size and the mounting system of the head rendered this impossible.

With these restrictions in mind, an indirect approach to the problem was pursued. This involved the measurement of the single scattered spectrum at a particular angle and, by making the appropriate corrections, going from this to the unscattered or output spectrum. This approach has the advantage that each scattering angle will yield a different scattered

spectrum, but the primary spectrum deduced from each should, of course, be the same. Thus, any variation in the calculated primary spectrum would immediately indicate a flaw in the method. Since the region of interest in the spectrum is that below about 800 Kev, i.e. the tail energies, the spectrum was divided into two parts, viz: tail and peak. The area under the peak of the once-scattered spectrum was measured in order to provide a comparison between the amount of primary radiation and the amount of degraded radiation. The tail of the spectrum was the only region studied in detail. The peak area of the scattered spectrum was related to the peak area of the output spectrum through the appropriate scattering equations, so that the tail of the primary spectrum could be expressed in terms of photons per primary photon per Mev.

APPARATUS

The scintillation spectrometer employed in this experiment made use of a NaI(Tl) crystal. This was cylindrical in shape and had a diameter of 2" and a depth of 2". Mounted directly onto the end of this crystal was a similar, non-activated NaI crystal of the same size. The purpose of this second crystal was to reduce the size of the backscatter peak that normally arises from the face of the photomultiplier tube. A Du-Mont 6363 photomultiplier tube was optically coupled to the crystal. This coupling was achieved by using Nuclear Chicago D.C. 200 optical coupling fluid, between the faces in contact. Since the face of the 6363 tube has a diameter greater than that of the crystal, an aluminum shim was constructed to ensure the tube and crystal formed a rigid unit. Optically opaque tape was then wound around the system from the base of the tube to the end of the crystal, and it was housed in a lead container, as shown in diagram 1. The container was mounted onto a frame which provided a rigid support for the system. The frame was on wheels and could readily be moved from place to place (diagram 2). The lead shielding was of such a thickness that background radiation was reduced to a manageable amount. This thickness was 3.5" at the crystal. In addition, lead blocks were placed on a platform on the source side of the frame to increase the shielding. These blocks were about 5" square and 10" long. Radiation was admitted to the crystal through a collimator 10" long and 1/4" in diameter. This collimator could be removed, if necessary, and smaller ones substituted. The front of the frame could be raised on a pivot so that the front wheels were clear of the floor, and the whole unit could then be rotated about the pivot axis. The line of sight of the collimator intersected the pivot axis.

APPARATUS

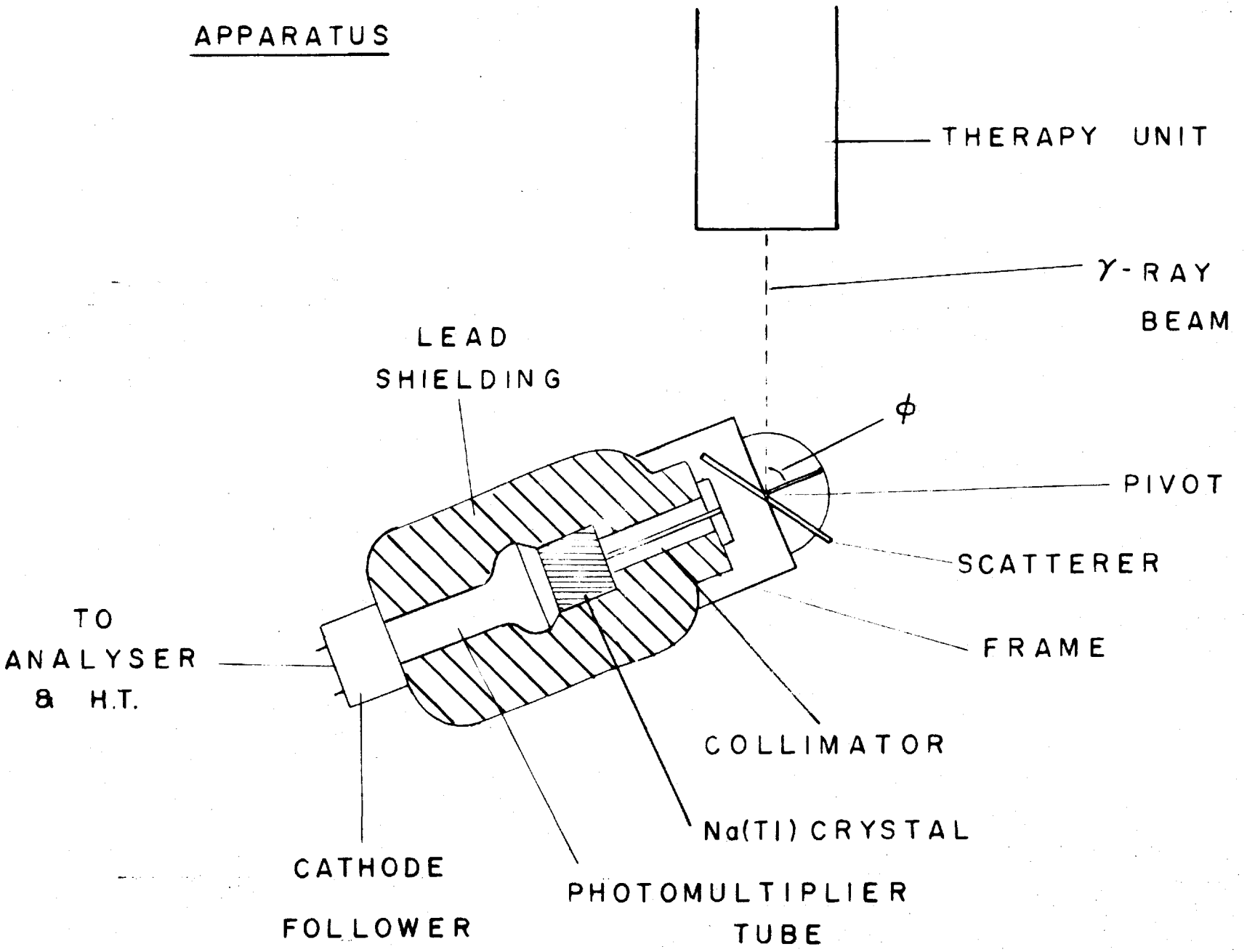

DIAGRAM 1 - Diagram of Apparatus

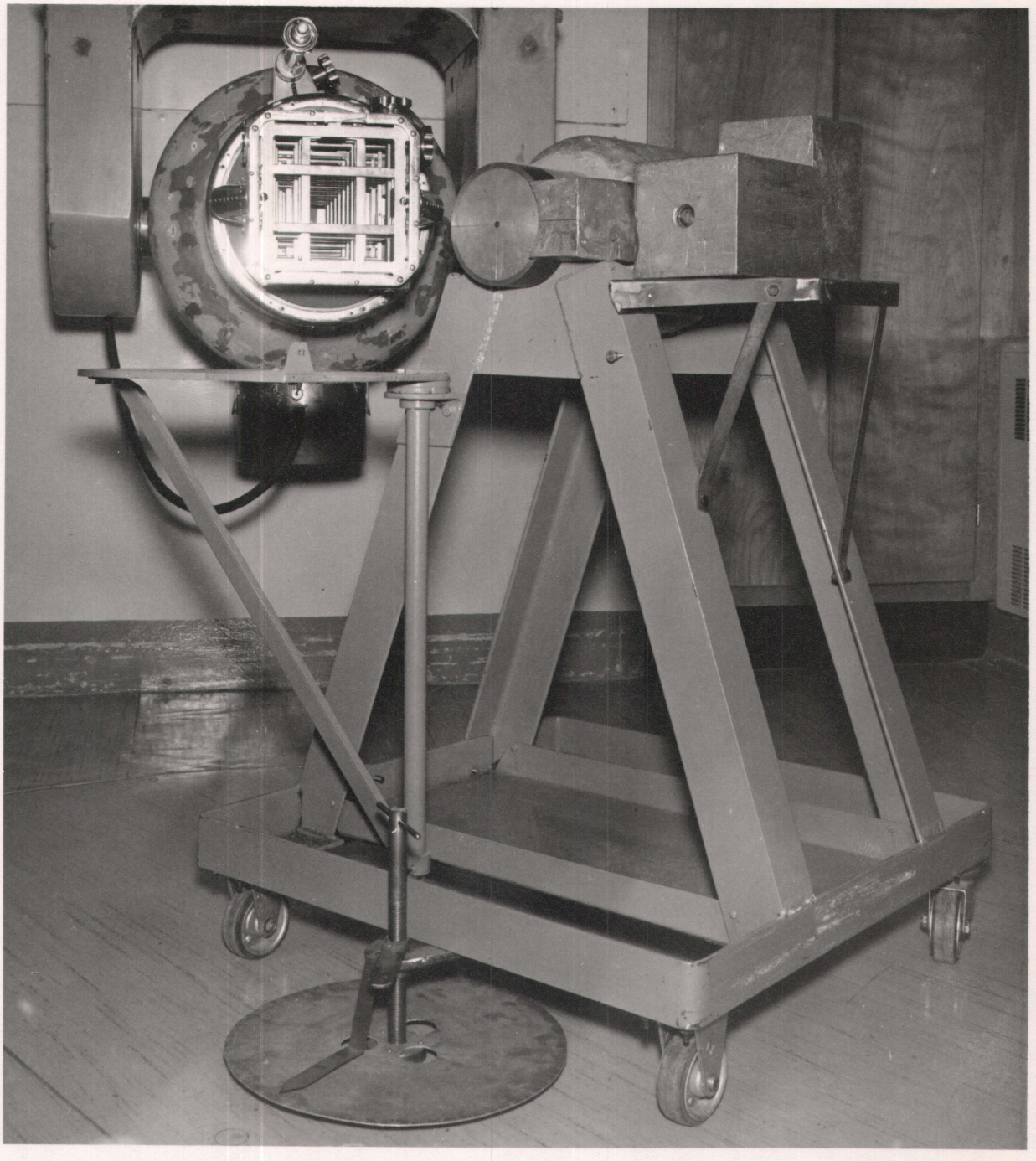

DIAGRAM 2

Photograph of Apparatus

The scattering slab was suspended in the γ-ray beam in such a position that it could be "seen" by the crystal. This slab consisted of a piece of lucite, 7" x 5" x 1/16", attached to the end of an aluminum rod. A bar on the therapy head could be moved beyond the end of the beam defining system by means of a rack and pinion, and the rod was attached to this with a right angle clamp, so that the scatterer hung down in the beam. The position of the scatterer with respect to the source could be accurately determined, as the bar on the head moved past a fixed scale. The head and scattering slab could then be moved back and forth as a unit until the irradiated section of the lucite was in the line of sight of the detecting system. The orientation of the slab with respect to the beam direction and detector line of sight was found not to be critical. The usual orientation was to bisect the angle between beam and detector with the slab. The pulses from the photo-multiplier tube were fed into a cathode follower which was mounted directly behind the tube as shown in diagram 3. The electronic apparatus after the cathode follower was mounted inarack which was situated outside the therapy room. Pulse and H.T. cables were led to the detecting unit. The pulses from the cathode follower were amplified by a Baird-Atomic non-overloading linear amplifier (Model 215), and were analysed by a single-channel pulse height analyser (B.A. Model 510). A Marconi scale of 10 scaler was used, which was controlled by a time clock. A high voltage power supply (B.A. Model 312) was used to supply the H.T. for the phototube.

CIRCUIT DIAGRAM

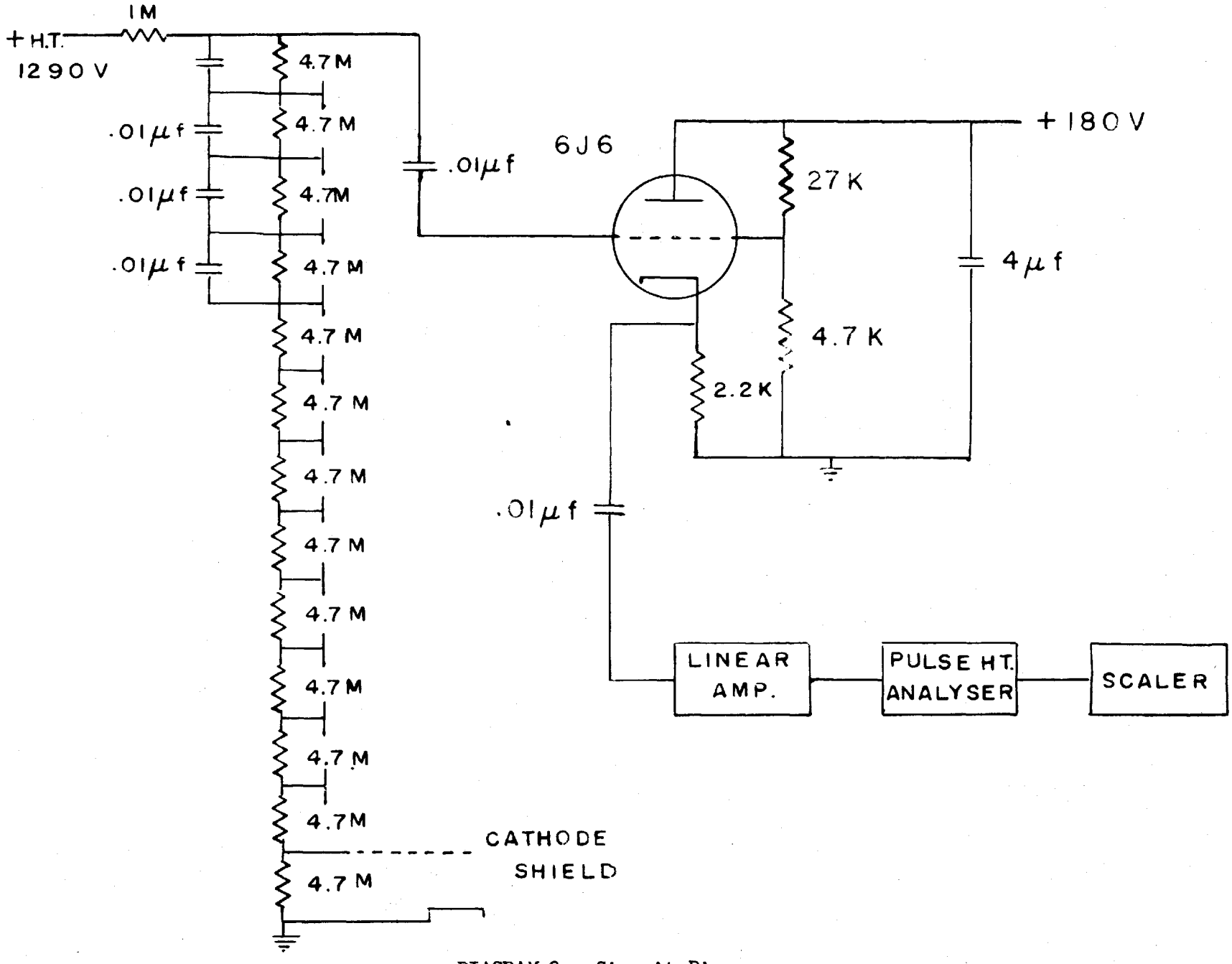

DIAGRAM 3 - Circuit Diagram

ALIGNMENT

The angle between the line of sight of the detector and the beam from the therapy unit is of considerable importance, since it is the scattering angle, φ , in question. It was measured on a protractor disc mounted on the frame pivot. When the pivot is screwed down, the protractor is fixed with respect to the floor and a pointer, rigidly fixed to the frame, passes over it. However, when the pivot is clear of the floor, the disc can be rotated to the desired position (see diagram 4). The disc was divided into one degree intervals from 0-359°.

When the beam and detector were exactly aligned, the disc was set to read 0°. This alignment was carried out by first positioning the pivot. A light in the ceiling of the therapy room projects a pair of cross hairs onto the floor. This indicates the axis of rotation of the turn-table used for rotation therapy. The centre of the top of the pivot was positioned at the intersection of the cross hairs from the ceiling light. The pivot was then screwed down in order to fix its position (diagram 4). The Saskatoon teletherapy unit contains beam indicator lights. The point of intersection of two filament images defines a point 80 cm from the source, and at the centre of the beam (diagram 5). The unit was moved longitudinally until the images of these filaments fell on the end of the detector collimator, as shown in diagram 5(b). When the detecting unit was exactly in line with the beam, the hole of the collimator was mid-way between the two filaments. If the frame was rotated one way or the other from this position, then the filament images moved with respect to the hole and the latter could be seen to be displaced towards one of the images. This

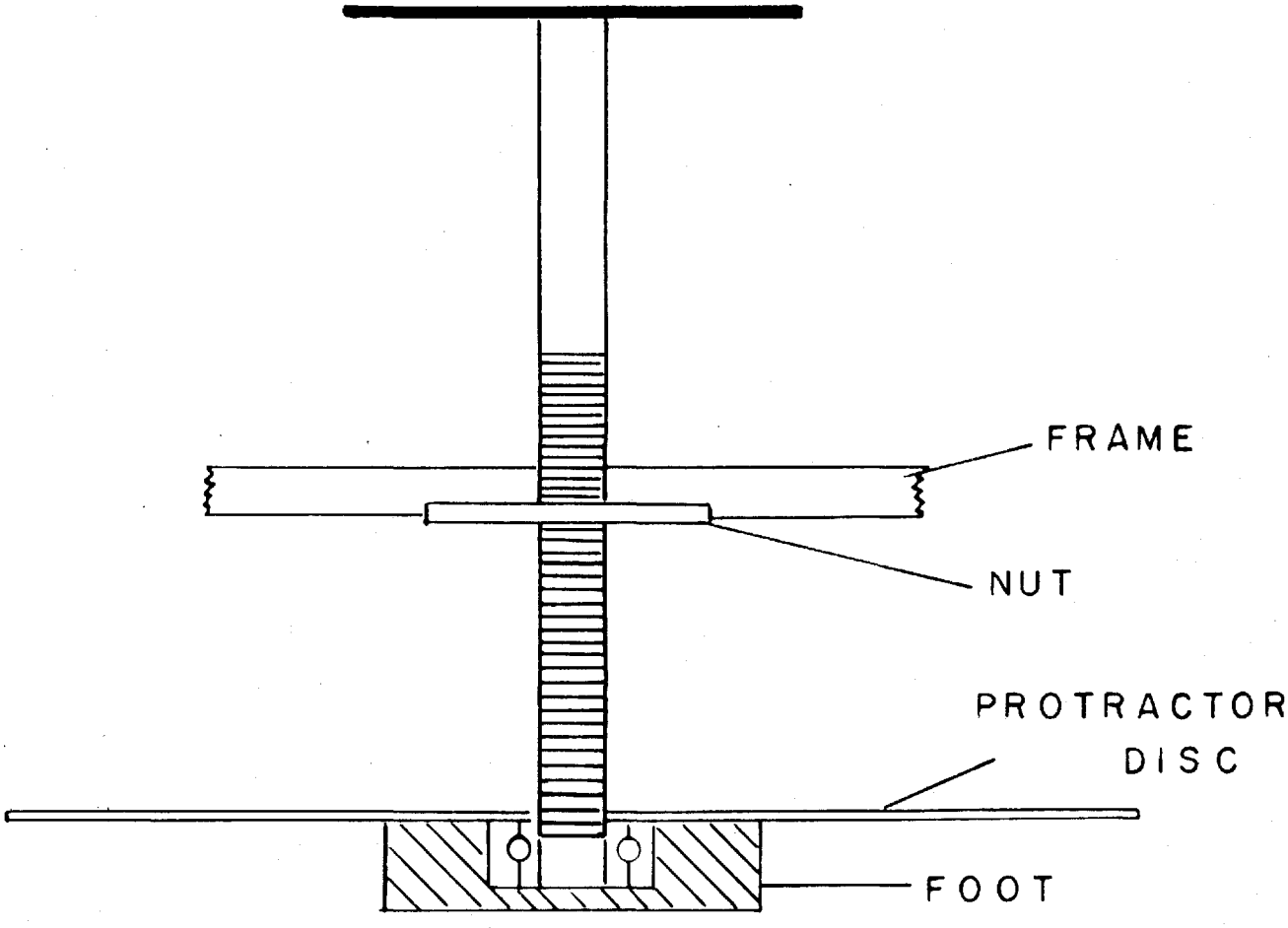

DIAGRAM 4 - Pivot Arrangement

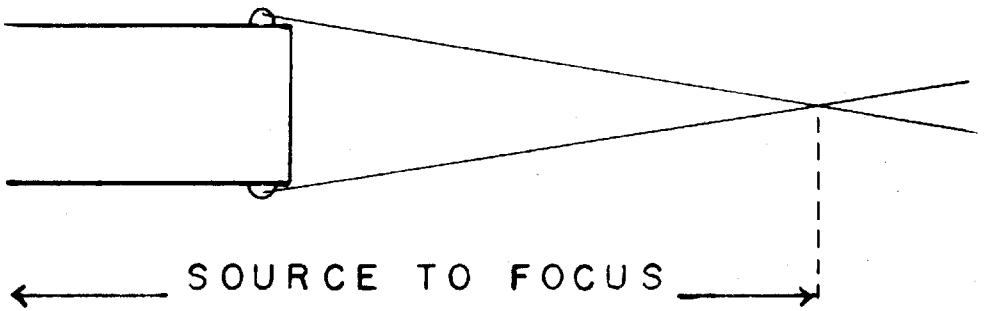

(a)

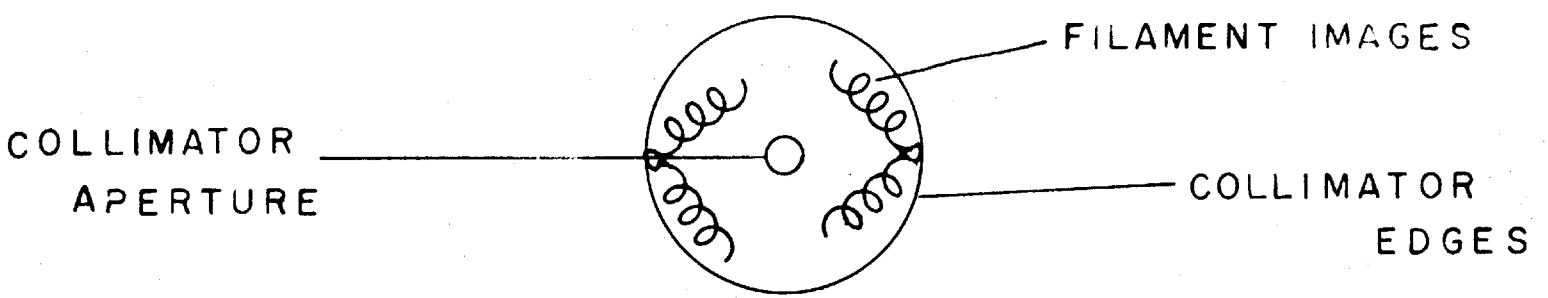

(b)

DIAGRAM 5 (a)(b) - Alignment System

technique was sufficiently sensitive to give a zero setting to within $\pm 1^{o}$.

To facilitate subsequent alignment procedure, the frame was first positioned and aligned as described above. A long arm was then bolted onto the frame, and the point at which it touched the floor was marked. For further experiments, it was then only necessary to locate the pivot by means of the ceiling light, and then rotate the frame until the arm came around to the marked point on the floor. The pivot was then raised in order to release the protractor disc, and the latter was rotated to read zero. The pivot was screwed down, fixing the disc, and any further frame orientations could be read in terms of an angle with respect to the beam.

THEORY

The general theory of scintillation spectrometry is now well established. (Ref. 1-4) Standard methods were employed in these experiments.

The radiation from the therapy unit which is incident on the scattering material will undergo Compton scattering as the principal interaction process. If the slab is thin enough, then most of the photons will suffer only one scattering before they leave it. Only photons which are scattered through the angle which the beam makes with the detector, φ, will be seen by the crystal. The spectrum of radiation entering the crystal will then be distorted in a number of ways. Some of the more energetic photons will pass right through the crystal without interacting. As this is more probable with high energies, this region of the spectrum will be reduced with respect to the low energy end. Other photons will undergo photoelectric absorption in the iodine, and the resulting K X-ray may escape. Such escape gives rise to pulses corresponding to an energy 28 Kev below the incident photon energy. Those photons which are scattered in Compton interactions may, after one or more scatters, escape from the crystal and give rise to pulses corresponding to reduced energies.

The above distortions were corrected by using a correction matrix described in Appendix I. In addition, there exist other smaller distortions which, in this work, have been ignored. These are backscatter from the face of the phototube and escape of electrons. Besides these crystal distortions, the photomultiplier tube imposes a gaussian spreading on all parts of the spectrum. This distortion is considered in the correction matrix. However, it has little effect on spectral shape for the lower photon energies. The associated electronics may also have a small effect on the spectral shape.

By using the correction matrix, it was possible to convert the

measured scattered spectrum to the true scattered spectrum. It was then necessary to modify this to yield the spectrum which was incident on the scatterer, i.e. the output spectrum of the therapy unit. If E'' is the energy of a pulse as obtained from the analyser, then the measured spectrum of N(E'') vs E'' will give a distribution such as shown in diagram 6(a). When this spectrum is corrected with the matrix, we have the spectrum which emerged from the scatterer. This has the form shown in diagram 6(b), where k' is the energy of the scattered photon, and N(k') is the number of scattered photons per Kev per second. The peak occurs at a value of k' corresponding to a photon of average energy 1.25 Mev scattered through an angle φ. In fact there are two energies scattered through this angle, but these are not resolved in the scattered peak. It is desired to deduce the incident spectrum which generated this scattered spectrum, and which will be of the form shown in diagram 6(c). As stated above, only the area under the peak is considered and no resolution of the two primary photon energies is possible.

The incident and once-scattered spectra may be related as follows:

$$N(k')dk' = N(k)dk \frac{d_e\sigma}{d\Omega} n \qquad (1)$$

where $\frac{d_e\sigma}{d\Omega}$ is the Klein Nishina scattering cross section per electron, and n is the number of electrons in the relevant scattering volume.

Now, from the Compton relationship we have

$$k' = \frac{k}{1 + \frac{k}{\mu} \operatorname{vers} \varphi} \quad \text{where } \mu = m_o c^2 \qquad (2)$$

whence

$$\frac{dk'}{dk} = \frac{k'^2}{\mu^2} \left(\frac{\mu}{k'} - \operatorname{vers} \varphi \right)^2 \qquad (3)$$

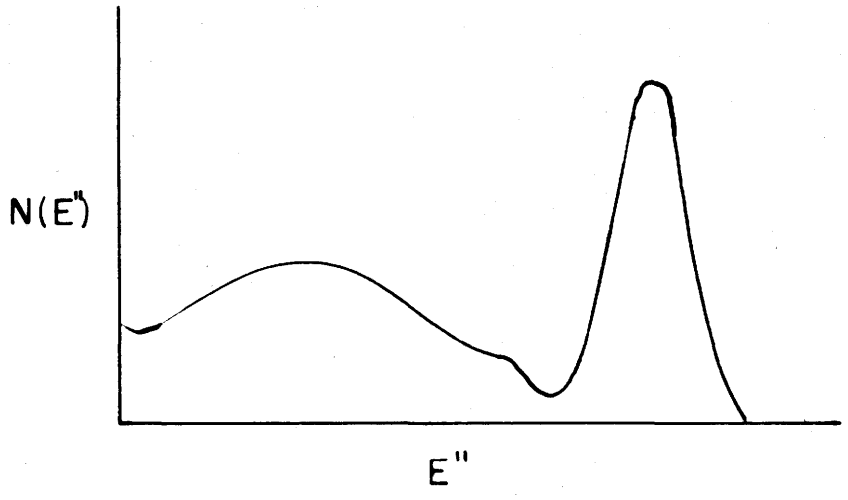

(a)

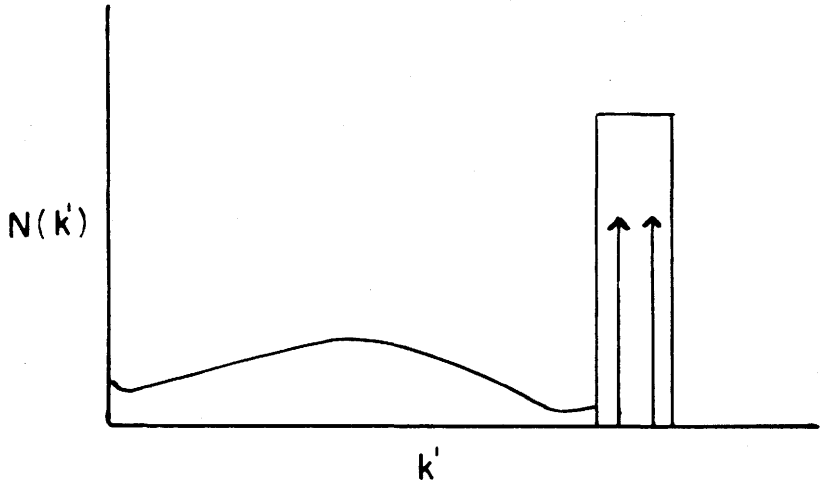

(b)

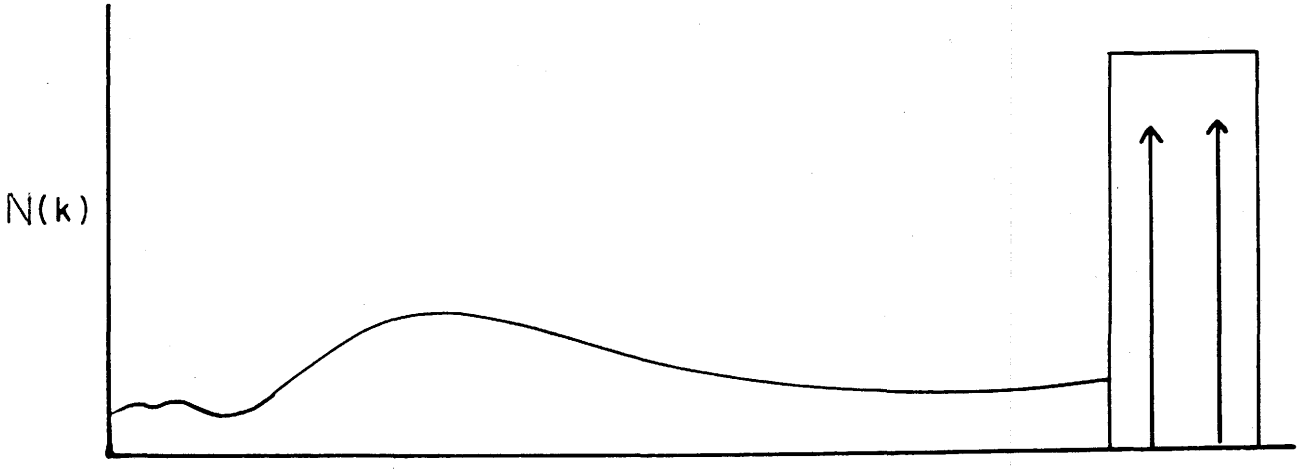

(c)

DIAGRAM 6 (a)(b)(c) - Modification of Spectra

The term, $\frac{d_e\sigma}{d\Omega}$, accounts for the fact that lower energy photons in the primary spectrum will be subject to a greater scattering cross section for any particular angle φ, and consequently that this region would be enhanced in the scattered spectrum. The Klein Nishina formula may be given by

$$\frac{d_e\sigma}{d\Omega} = \frac{r_o^2}{2} \frac{1}{(1+\alpha \text{vers}\varphi)^2} \left\{1 + \cos^2\varphi + \frac{\alpha^2 \text{vers}^2\varphi}{1+\alpha \text{vers}\varphi}\right\} \qquad (4)$$

In this equation, $r_o = \frac{e^2}{m_o c^2}$ is the classical electron radius, $\text{vers}\varphi = (1 - \cos\varphi)$, and $\alpha = \frac{h\nu}{m_o c^2}$.

Substituting this in equation (1) yields

$$N(k')dk' = N(k)dk \frac{r_o^2}{2} \frac{1}{(1+\alpha \text{vers}\varphi)^2} \left\{1 + \cos^2\varphi + \frac{\alpha^2 \text{vers}^2\varphi}{1+\alpha \text{vers}\varphi}\right\} n$$

Thus, N(k), the number of photons per Kev per second in the output spectrum, is given by

$$N(k) = N(k') \frac{dk'}{dk} \frac{2}{r_o^2} \left\{ \frac{(1+\alpha \text{vers}\varphi)^2}{1 + \cos^2\varphi + \frac{\alpha^2 \text{vers}^2\varphi}{1+\alpha \text{vers}\varphi}} \right\} \frac{1}{n}$$

If the expression for $\frac{dk'}{dk}$ is substituted, from (3)

$$N(k) = N(k') \left\{ \frac{k'^2 \left(\frac{\mu}{k'} - \text{vers}\varphi\right)^2}{\mu^2} \right\} \left\{ \frac{(1+\alpha \text{vers}\varphi)^2}{1 + \cos^2\varphi + \frac{\alpha^2 \text{vers}^2\varphi}{1+\alpha \text{vers}\varphi}} \right\} \frac{2}{n r_o^2}$$

The quantity $\frac{2}{n r_o^2}$ is a constant, and since we are not concerned with absolute magnitudes, it can be ignored. The rest of the equation contains quantities dependent on φ, and must be considered in the evaluation of N(k).

The area under the peak may be considered as representing a

number of photons. If this area is measured with a planimeter, then it can be represented as a rectangle of such a width and height that their product yields the original area. As will be discussed in a later section, the width of this rectangle is determined by the mesh of the correction matrix, and the appropriate height may be obtained. Since we are now dealing with an area under the peak rather than with an ordinate reading, the factor $\frac{dk'}{dk}$ is not applied. If $P(k')$ is the area of the rectangular peak in the scattered spectrum, then this may be related to the area of the corresponding peak in the output spectrum, $P(k)$, by the expression

$$P(k) = P(k') \frac{d\Omega}{d_e\sigma} \frac{1}{n}$$

or

$$P(k) = P(k') \left\{ \frac{(1 + \alpha \operatorname{vers} \varphi)^2}{1 + \cos^2\varphi + \frac{\alpha^2 \operatorname{vers}^2 \varphi}{1 + \alpha \operatorname{vers} \varphi}} \right\} \frac{2}{n r_o^2}$$

The tail of the output spectrum may be expressed in terms of photons per primary photon per Mev by dividing the ordinate values of the tail $N(k)$ in diagram 6(c) by $P(k)$.

CALIBRATION

In order to convert the abscissa scale of the graph of $N(E'')$ vs E'' from base line volts, as read on the pulse height analyser, to actual photon energies, the analysing system must be calibrated. This was done by employing a number of γ -ray sources which had well-defined characteristic decay energies. The base line voltages corresponding to these energies were found in each case, and a calibration curve was drawn, as shown in diagram 7, with base line volts plotted against energy. The sources used were Co^{60}, with energies of 1.33 and 1.17 Mev, Cs^{137} with a single energy of .661 Mev and I^{131} with energies of .364 and .08 Mev. As can be seen in the graph, the points fell quite well on a straight line.

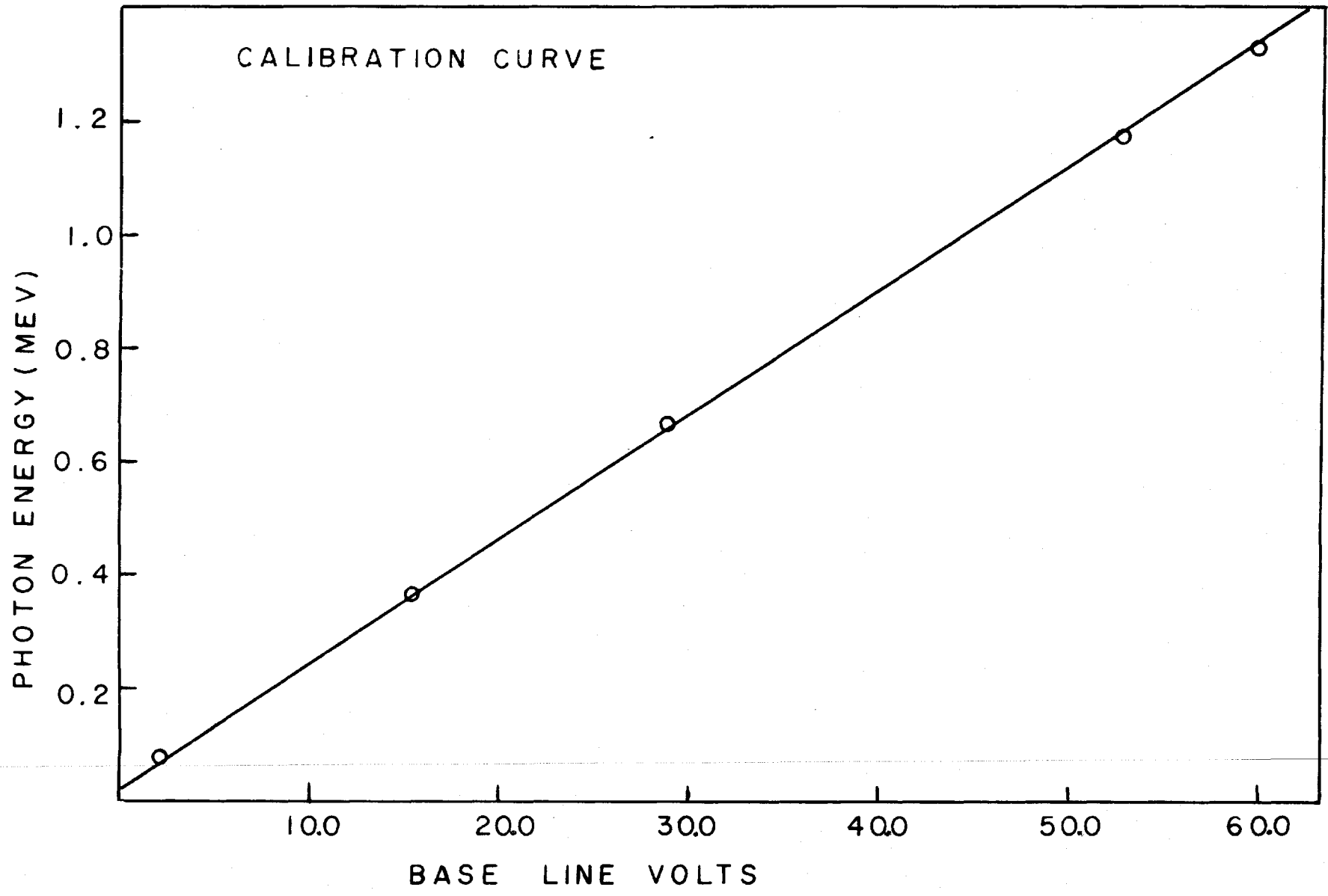

DIAGRAM 7 - Calibration Curve

MEASUREMENT OF SPECTRA

The apparatus was arranged as shown in diagram 1. The correction matrix for the detecting system contained intervals which varied as the square root of photon energy, thus providing more detail in the low energy region. To ensure that the peak of the scattered spectrum fell at a convenient point, with regard to the matrix, scattering angles φ were chosen to yield a scattered peak in the centre of a matrix interval. From the Compton relationship, we have

$$\cos\varphi = 1 - \frac{(k - k')\mu}{k'k} ,$$ where k is the incident energy, k' the scattered energy, and φ the scattering angle. If we assume that the two cobalt energies can be approximated by a single energy of 1.225 Mev, then to have, for example, a scattered peak at 841 Kev, i.e. $(29\sqrt{\text{Kev}})^2$ we must have

$$\cos\varphi = 1 - \frac{1225 - 841}{(841)\ (2.4)} , \quad \text{or} \quad \varphi = 36.8^{\circ}$$

The pivot of the frame was first positioned at the centre of rotation of the turn-table. This point was located by means of the overhead light as described in the alignment section above. The apparatus was aligned, and the graduated disc set to read zero. The frame was then raised on its pivot, and rotated to the desired angle. The electronic apparatus was warmed up for about three hours prior to a run. This was considered necessary, since there existed a considerable upward drift in the gain in the first two hours after switching on. This was probably due mainly to photomultiplier tube drift. A small Co^{60} source which could be fitted into

the end of the detector collimator was used for calibration. This source had an approximate strength of 2 millicuries, and was thus strong enough to give well-defined peaks, in a counting period of 15 seconds. After the warm-up time, the gain of the linear amplifier was adjusted so that the Co^{60} peak, at 1.33 Mev, fell at 60 V on the base line setting of the pulse height analyser. This enabled the calibration curve obtained earlier to be used. Counts within a 1.5 volt channel were taken at base line settings about half-way down the sides of the peak, where the counting rate is very sensitive to changes in peak position.

After the peak had been set, the scattering slab was placed in the beam. The beam-defining system on the Saskatoon therapy unit permits the beam, as seen at 80 cm from the source, to be continuously varied on both sides of a rectangle from 20 cm x 20 cm to 4 cm x 4 cm (ref. 5). In these experiments, the smallest field size was used throughout, in order to minimize background effects. A metal probe which could be fitted into the aperture of the detecting collimator was used to indicate the line of sight of the detector. The scatterer was positioned such that the detector locked at the centre of the irradiated region. In order to see if any variation in spectrum existed across this region, rough spectra were measured at a number of points from one edge to the other. The spectral shape was found to be constant except at the extreme edges. It was also found that the orientation of the scatterer with respect to the beam and detector directions had no noticeable effect on the shape of the spectra. However, for consistency, the scatterer was always arranged such that it bisected the angle between the beam and the detector line of sight.

To ensure that the scattering slab was thin enough to give a negligible amount of multiply scattered radiation, a series of slabs of different thicknesses were used in the measurement of spectra at a particular value of φ. Up to a thickness of about three times that of the lucite sheet subsequently used (1/16"), the shapes of the spectra were seen to be constant (diagram 8) and it was therefore assumed that the spectrum was essentially due to single scattering.

With the apparatus aligned and the gain of the amplifier suitably adjusted, the Co^{60} beam was switched on, and the counting rates in 1.5 volt channels covering the entire single scattered spectrum were determined. Counts were taken for half-minute intervals, and the counts obtained in this time were high enough to give reasonable statistical accuracy ($\pm$ 5%). When the run was completed, the stability of the apparatus was checked by locating the position of the 1.33 Mev Co^{60} peak, using the small cobalt source referred to above.

The scatterer was then completely removed from the beam, and a background run was taken using the same intervals as before. A further stability check was carried out at the conclusion of the background run.

The difference between the two scans gave the raw measured spectrum which was corrected as described in the following section. For the smallest values of φ the background approached 50% of the total counts in the low energy region, as can be seen in Table 1. However, at higher energies, and for greater scattering angles the background was generally less than 15% of the gross counting rate.

For all spectra a number of points were repeated, particularly where doubtful readings occurred. This procedure tended to reduce variations

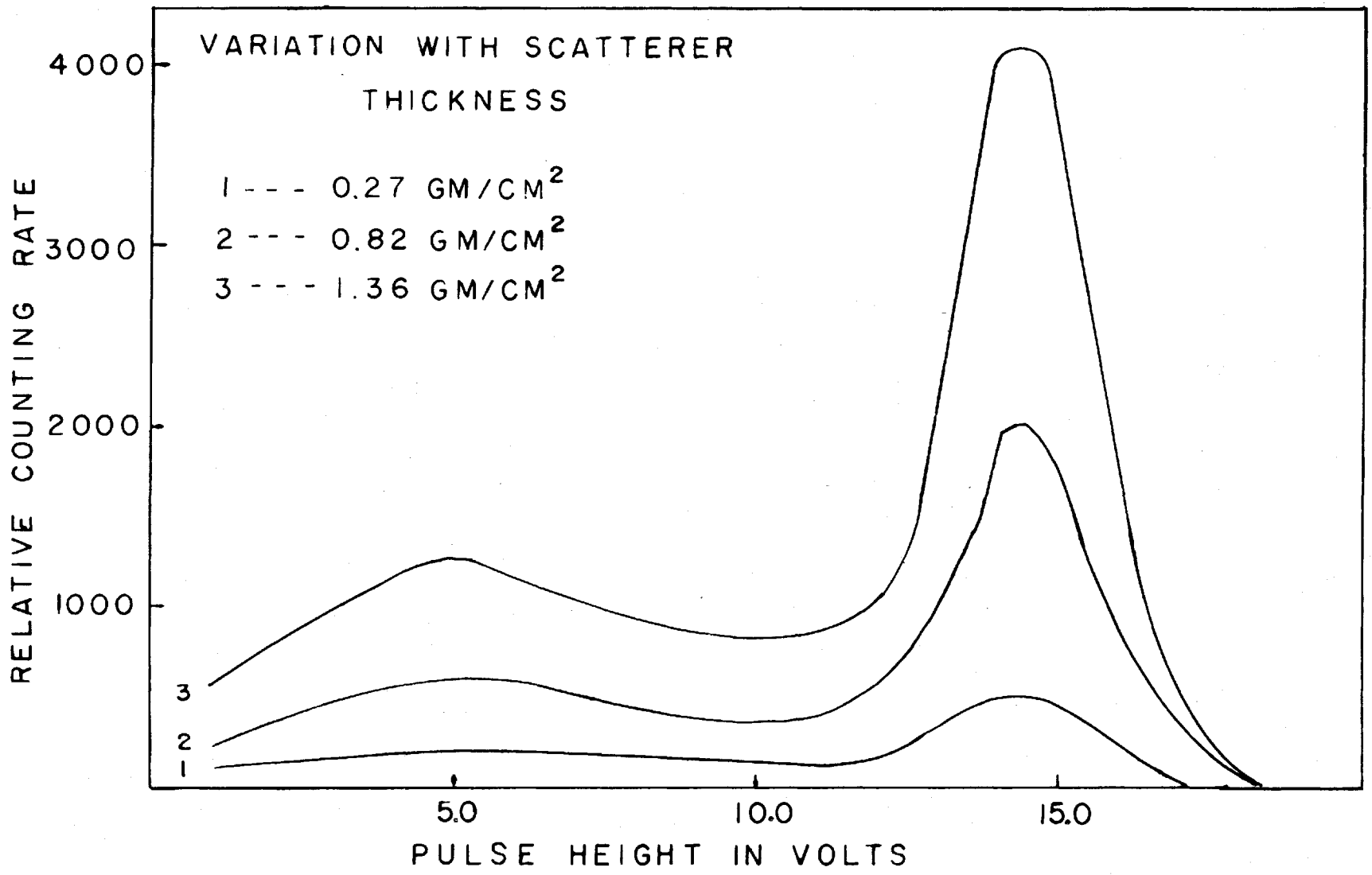

DIAGRAM 8 - Variation of Single Scatter Spectrum with Scatterer Thickness

TABLE 1

TABLES OF RAW DATA FOR LARGE AND SMALL ANGLES

$\varphi = 111^\circ$			$\varphi = 54^\circ$		
Base Line Volts	Counts per 15 sec	Back-ground	Base Line Volts	Counts per 30 sec	Back-ground
10	412	125	10	738	266
20	486	106	30	856	316
30	688	128	50	1089	406
40	948	150	70	1239	373
50	1315	163	110	950	278
60	1282	161	150	751	222
70	1101	190	170	521	216
80	993	188	210	373	177
100	1086	147	250	770	157
110	2504	166	270	1546	174
120	3683	172	290	904	171
130	1982	104	330	131	144
150	109	81			

in spectra produced by statistical fluctuation.

In order to test reproducibility, the spectra for a number of angles were repeated on separate occasions. The counting rate from the scatterer and the background values were found to be reproducible to about 5%.

TREATMENT OF DATA

Graphs were plotted of net counting rate versus B.L.V. The abscissa of these graphs were converted to energy units by means of the calibration curve. For the purposes of the matrix, ordinate readings at odd values of z were taken from the graphs, where $z = (E'')^{1/2}$ and E'' is the scattered photon energy, that is, values at z = 1, 3, 5 etc. (see diagram 6(a)).

Since $N(z)dz = N(E'')dE''$, and $z = (E'')^{1/2}$, it can be seen that

$$N(z) = N(E'')\ 2z$$

where N(z) is the number of pulses per unit interval of z. Thus in converting the spectrum from one in E'' to one in z, each ordinate reading must be multiplied by 2z. When this is done, the spectrum is then in a form which can be handled by the matrix (see Appendix I). The area under the peak in the unconverted spectrum, $N(E'')$ vs E'', was measured. The peak was cut off on the low energy side by dropping a perpendicular at the lowest point in the trough next to the peak. This area was then converted to a number of photons by comparing it to an area which represented a known number of photons. Since this area was then to be presented in histogram form, with a width of $2\sqrt{\text{Kev}}$, the area was divided by 2, to yield an ordinate reading for the peak. A column N(z) was thus obtained, as can be seen in Table 2. This table is a specimen operation on a measured spectrum to yield the final output spectrum N(k). The spectrum N(z) was then multiplied by the inverse matrix M^{-1} to yield the column N(y) where $y = \sqrt{k'}$. This column was then divided by 2z to give $N(k')$, and the peak value was multiplied by 2, to give a corrected scattered spectrum $N(k')$ vs k', the peak of the spectrum $P(k')$ being given as in $N(E'')$ by an area, representing

TABLE 2

CONVERSION FROM N(E'') TO N(k)

$\varphi = 90.5^{\circ}$

E''	Z	N(E'')	2ZN(E'') =N(Z)	N(y)	$\frac{N(y)}{2Z}=N(k')$	k'(Kev)	k(Kev)	N(k)	N(k)/P(k)
1	1	3.6	7.2	3.1	1.6	1	1	1.61	.18
9	3	3.5	21.0	8.7	1.4	9	9	1.44	.16
25	5	3.5	35.0	16.9	1.7	25	26	1.68	.19
49	7	3.4	47.6	31.4	2.2	49	54	2.20	.25
81	9	3.6	64.8	42.0	2.3	81	96	2.25	.25
121	11	5.1	112.2	90.3	4.1	121	160	3.78	.43
169	13	8.4	218.4	187.7	7.2	169	257	6.09	.69
225	15	6.0	180.0	175.6	5.8	225	396	4.41	.50
289	17	1.5	51.0	59.5	1.7	289	647	1.00	.11

PEAK

E''	Z	Area	$\frac{\text{Area}}{2}$	Cor- rected Height	Cor- rected Area	k'	k	P(k)
361	19	1550	775	1014	2028	361	1225	8872

a number of scattered photons. (see diagram 9)

The values of $\frac{dk'}{dk}$ and $\frac{d\Omega}{d_e\sigma}$ were then evaluated as given in the theory, and each value in the tail of N(k') was multiplied by both of these, to give a corresponding N(k) (see equation (1)). The peak was multiplied only by $\frac{d\Omega}{d_e\sigma}$, for reasons given above, and a final peak area P(k) was obtained.

The values of k corresponding to the measured k' were evaluated by using the Compton relation:

$$k = \mu\left(\frac{\mu}{k'} - \text{vers}\varphi\right)^{-1}$$

The output spectrum curves N(k) for various angles φ were normalized by dividing all the values of N(k) (see Table 2) by P(k). The tail values are then expressed as photons per Mev per primary photon.

DIAGRAM 9 - Effect of Matrix Correction

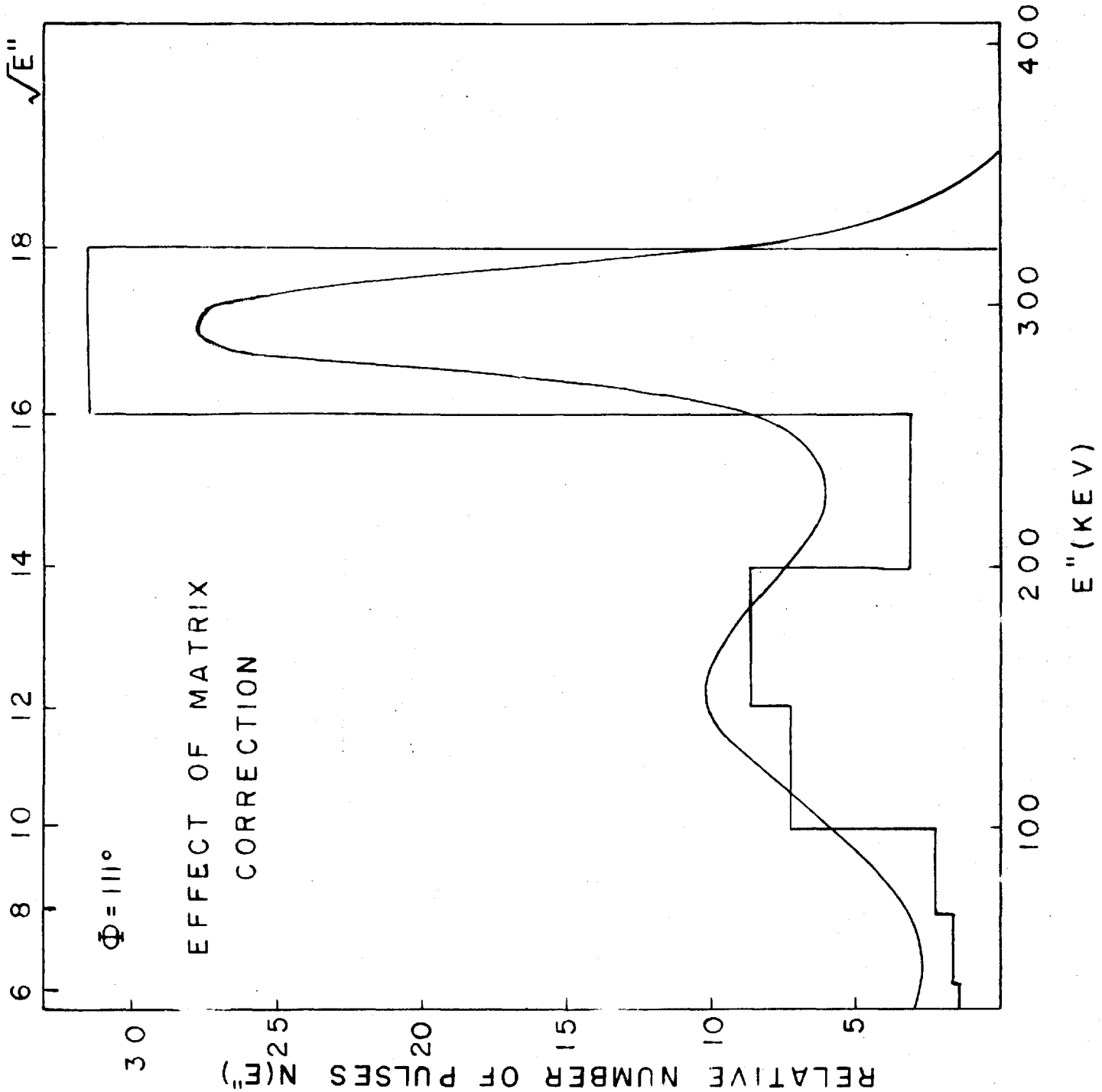

RESULTS

The five angles for which spectra were measured ranged from $\varphi = 111^{\circ}$ to $\varphi = 54^{\circ}$ (see diagram 10). The largest angle was dictated by the physical dimensions of the therapy head. The detecting unit was rotated until it was touching the head, and the largest applicable angle less than this was 111°. The minimum angle was governed principally by background considerations. At angles much nearer to the primary beam the background became too large with the existing shielding.

As can be seen in diagram 11, there is some variation in the output spectra from the various angles in the very low energy region. The background to signal ratio in the measured spectra was highest in this region, and the variance may be largely attributed to this. It is interesting to note, however, that all spectra exhibit a small peak at about 50 Kev. In view of the spread in the spectra in this region, it is difficult to say whether or not any significance can be attributed to this peak.

In general the five output spectra obtained from the various angles compare very favorably. They all have the same shape, with a peak at 250 Kev. The greatest variation in peak heights is less than 4% of the total height. Thus the results give confidence in both the method of analysis and the correction matrix.

A theoretical calculation of the low energy radiation generated in the source material and in the beam-defining system was carried out by Cormack & Johns (Ref. 6). In those calculations, a Co^{60} source 2.5 cm in diameter, and 1.25 cm thick, was considered. Those are the dimensions of the source in the Saskatoon unit used in the above experiment. First

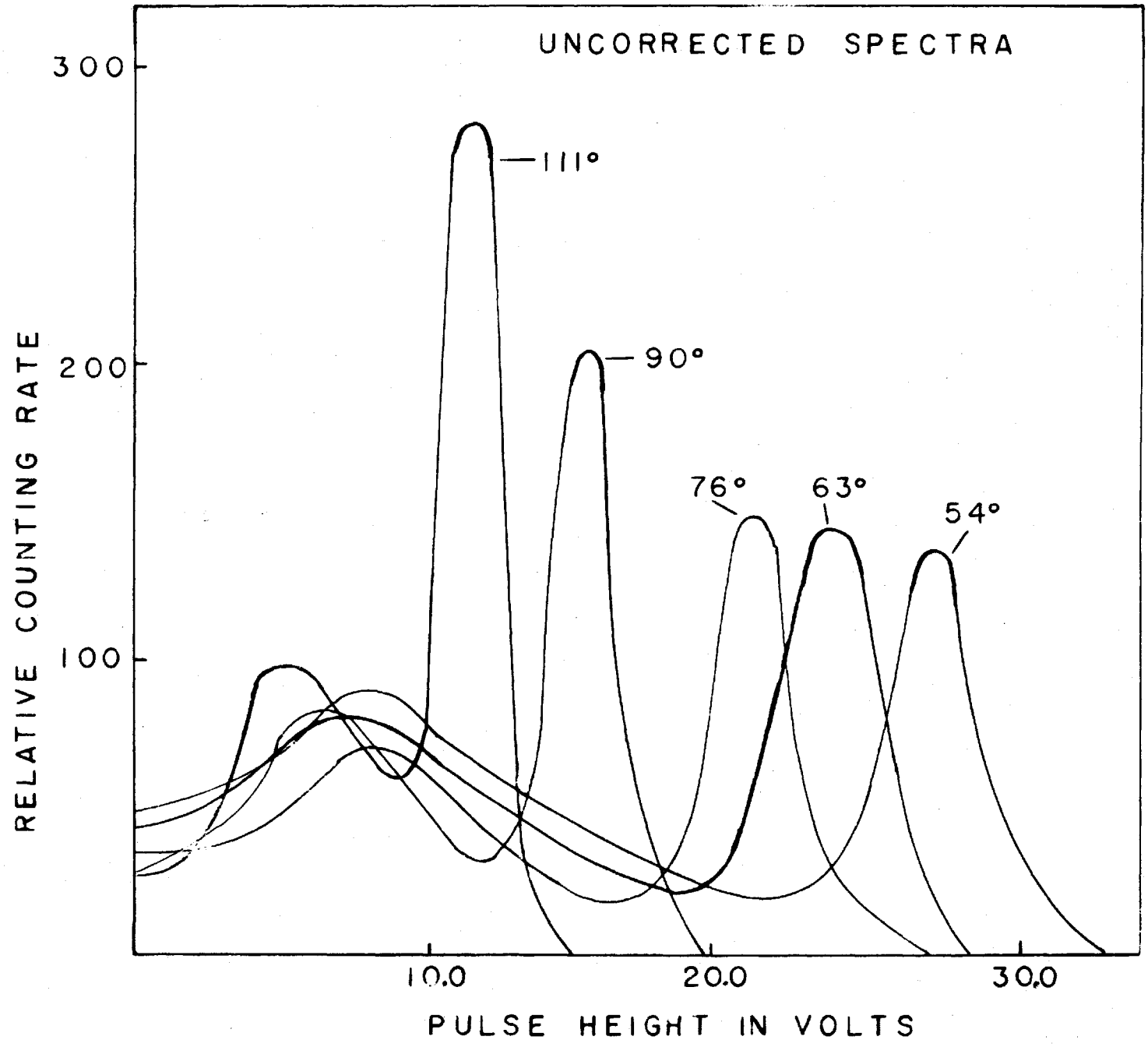

DIAGRAM 10 - Uncorrected Spectra

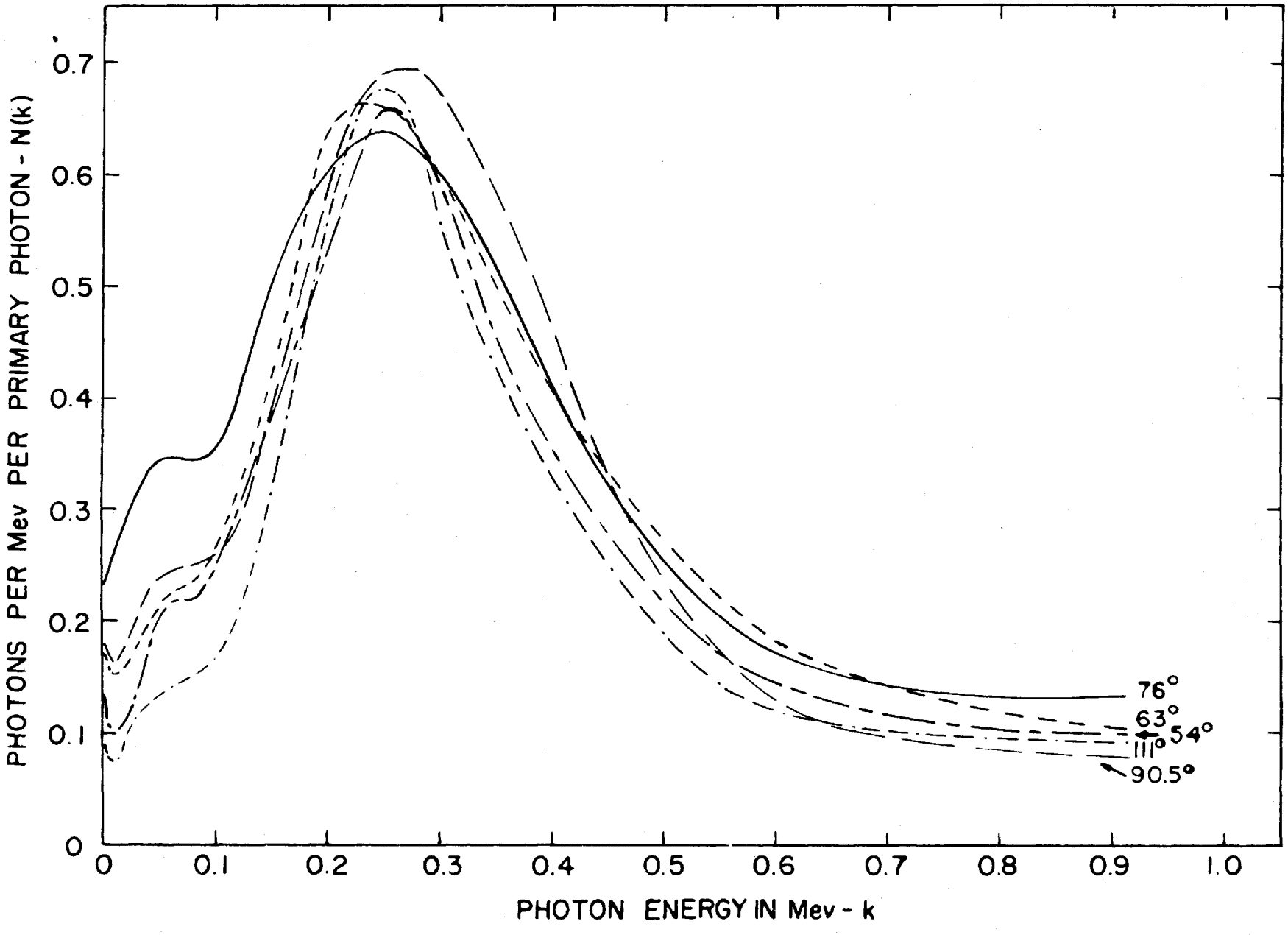

DIAGRAM 11 - Comparison of Output Spectra

the contribution from radiation originating within an axial cylinder and suffering a single scatter was evaluated. Then the single scatter from points not within this cylinder was calculated. The latter was more difficult due to the lack of symmetry, and certain approximations were made. For higher orders of scattering, the complexity of the problem increased, and further approximations were necessary. The sum of the above processes yielded the spectrum of radiation emerging from the source. The effects of the beam-defining system on this spectrum for various field sizes were also considered. It may be noted that this contribution did not change the spectrum significantly in the low energy region, e.g. below 400 Kev.

A comparison between the average of experimental results shown in diagram 11 and the theoretical results described above shows a remarkable similarity (diagram 12). Both spectra peak at the same energy and the peak heights agree within 5%. In view of the approximations made in the theoretical treatment, the experimental data is probably more reliable. The spectra obtained from the latter indicate some fine structure in the low energy region, and have less scattered radiation near the peak than the theoretical curve for scattering within the source. However, the differences are probably not significant and may be largely attributed to approximations in the theoretical treatment.

Some investigations were made into the effects on the output spectrum of variations in field size. Theoretically, the scatter contribution in the high energy region should increase. In the experimental results obtained, no significant increase was detected.

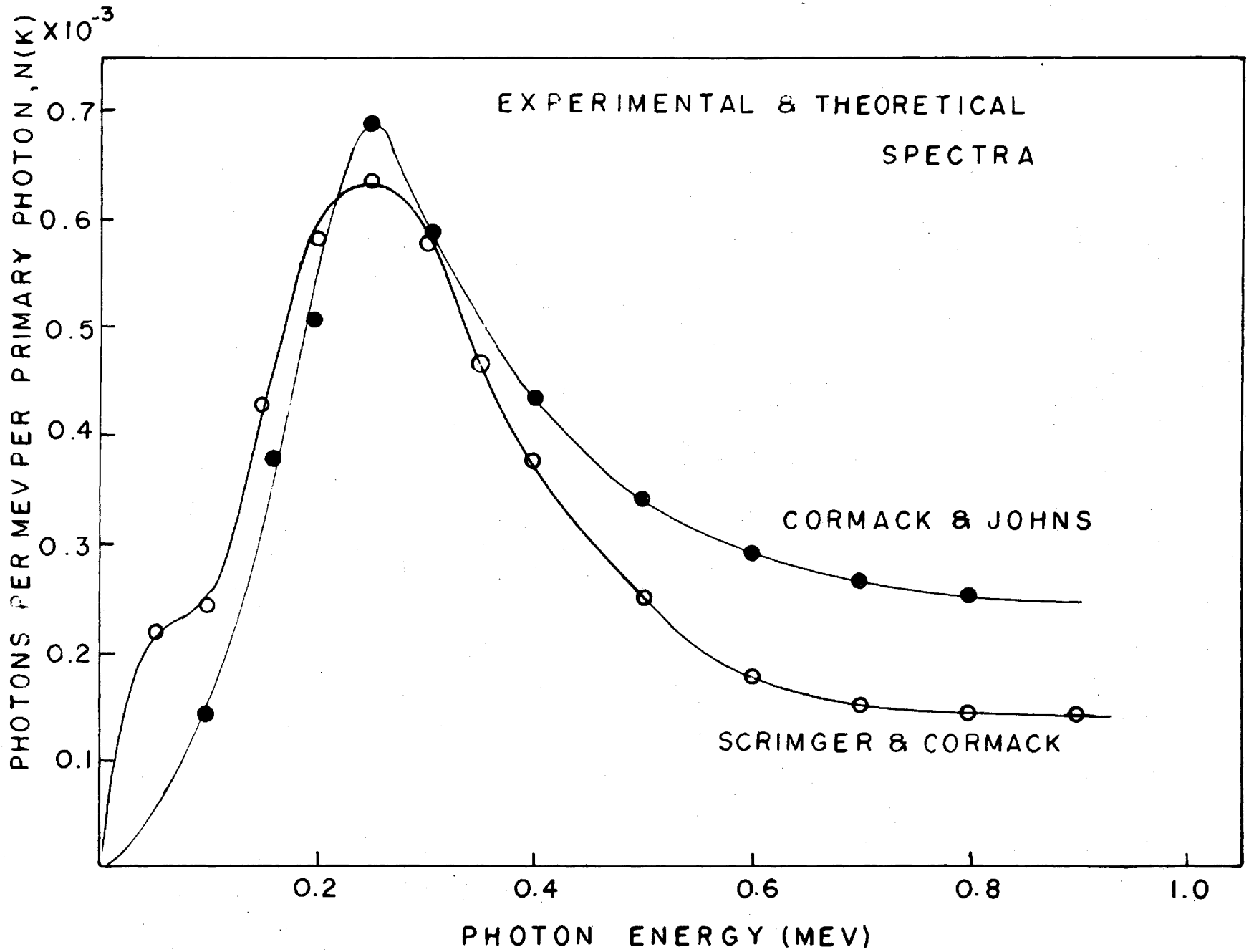

DIAGRAM 12 - Experimental and Theoretical Spectra

SUMMARY

The output spectrum of the Saskatoon Co^{60} teletherapy unit was obtained from a series of measured single scattered spectra. The primary beam was incident on a thin lucite slab, and the scattered spectra at various angles were measured with a scintillation spectrometer. These spectra were corrected with a matrix formulated from existing theoretical data. They were then modified by the scattering equations, to yield the output spectrum of the unit.

A comparison between theoretical and experimental output spectra shows very good agreement. The principal discrepancy between the two is in the region below 50 Kev, where both theoretical and experimental data are not very reliable.

APPENDIX I

When scintillation spectrometry is employed in the measurement of γ-ray spectra, the observed spectrum must be corrected for the distortions introduced by the crystal and photomultiplier tube. These distortions were outlined in the discussion of the theory.

Data for the response function of NaI(Tl) crystals of various dimensions are given in a paper by Berger & Doggett (Ref. 7). Such response functions give the measured pulse height distribution for various photon energies incident on the crystal. In this paper the distortions due to K-escape, Compton escape, crystal efficiency and gaussian spreading were calculated numerically using Monte-Carlo methods. Photon energies were chosen which corresponded to the characteristic energies of certain radioisotopes.

The response function $R(E,E'')$ for a given crystal may be written as

$$R(E,E'') = H(E,E'') + G(E,E''), \text{ where}$$

$H(E,E'')$ is the part of the response function contained in the tail, and $G(E,E'')$ the peak section. $H(E,E'')$ is the probability that an incident photon with energy E will give rise to an observed pulse height corresponding to an energy between E'' and $(E'' + dE'')$. In our work, the photon energy considered is that of the scattered photon, i.e. $E = k'$. The peak term $G(E,E'')$ was treated independently by Berger & Doggett, and since we were not interested in peak shape in this work, there were no corrections for spreading of the peaks made. In addition to this, inclusion of the broadened peak in the matrix would give terms beyond the diagonal, which would make the inversion process and subsequent application very much more difficult.

Berger and Doggett's data were presented in histogram form, an example of which is shown in diagram 13. The histograms for energies .279 Mev, .661 Mev, 1.17 Mev and 1.33 Mev were used in our work.

Since the matrix was required to cover a wide energy range, from 0-1.25 Mev, it was decided to follow the method employed by Hubbell (Ref. 8), and to make the mesh of the matrix proportional to the square root of the energy. This would yield a fine matrix in the low energy region, with the coarsest part in the high energies.

Let the square root of the photon energy E in Kev be y, then odd integral values of y running from y = 1 to 35 were chosen as the centres of the matrix intervals. These correspond to energies of 1, 9, 25 .... 1089, 1225 Kev with the corresponding bins going from 0-4 Kev, 4-16 Kev, etc. Similarly, values of $Z = E''^{1/2}$, corresponding to those of y were chosen, i.e. with Z = 1, 3, 5 .... 35. The values of $E/32\{H(E,E'')\}$ for energies E = .279, .661, 1.17 and 1.33 Mev were obtained from the histograms. For each odd bin (i.e. bins 1, 3, 5 etc.) a curve of $E/32\{H(E,E'')\}$ vs E was drawn on log-log paper, through the four values of E obtained above (diagram 14(a)). From these curves, the values of $E/32\{H(E,E'')\}$ corresponding to E's of 225, 289, 361 .... 1225 were obtained. A table was then formed of E vs bin number, in which the body contained values of $E/32\{H(E,E'')\}$ (diagram 14(b)). For each row of this table, i.e. for particular values of E, the bin numbers were converted to values of E'' through the relation E'' = E/32 x bin number, and the corresponding value in the body of the table was multiplied by 32/E. Curves were then drawn of H(E,E'') vs E'' for each value of E, as shown in diagram 14(c). From these curves the values of H(E,E'') for E'' = 1, 9, 25, 49 1225

DIAGRAM 13 - Specimen Histogram Response Function of NaI(Tl) Crystal (1 3/4" diameter x 2" deep)

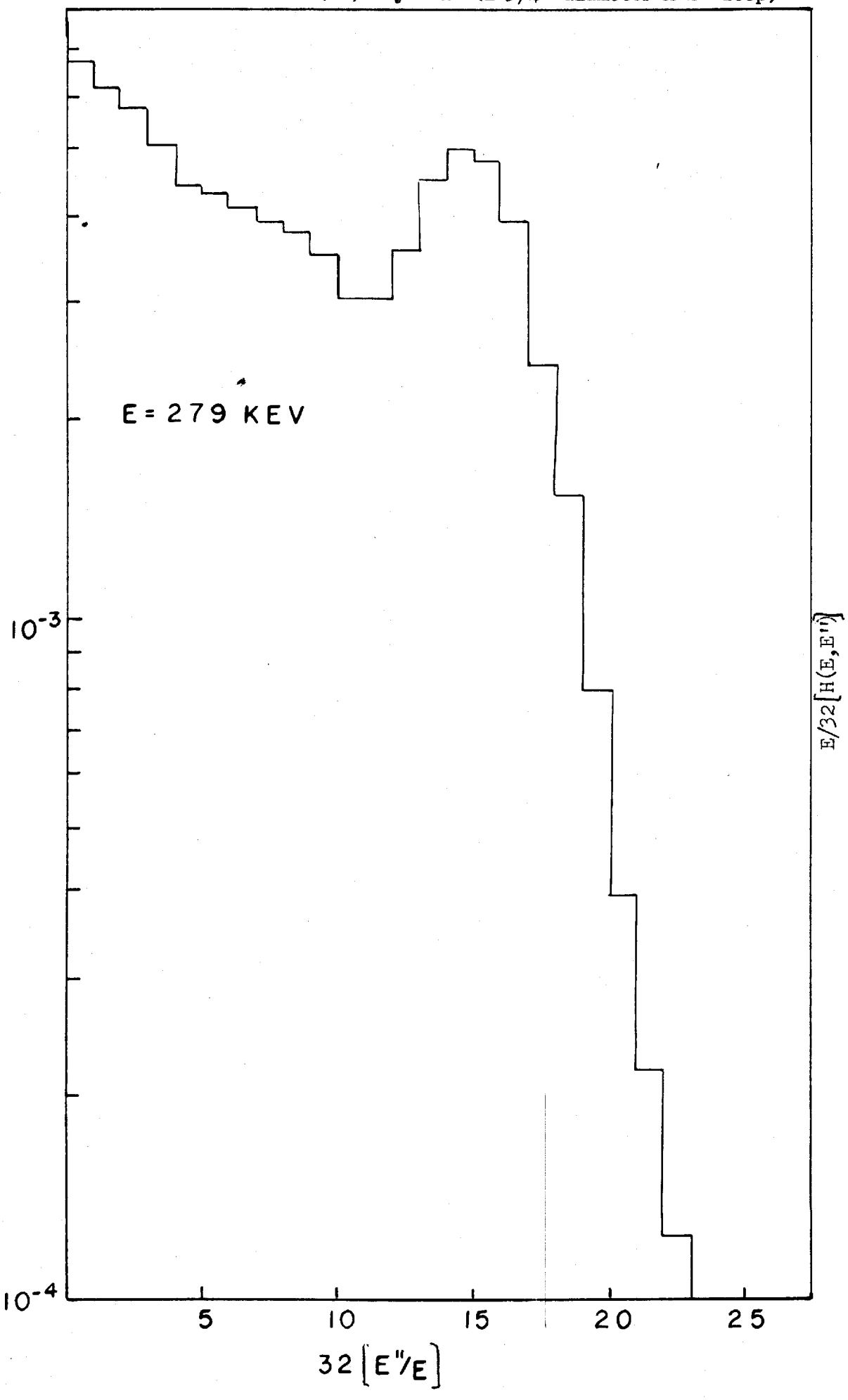

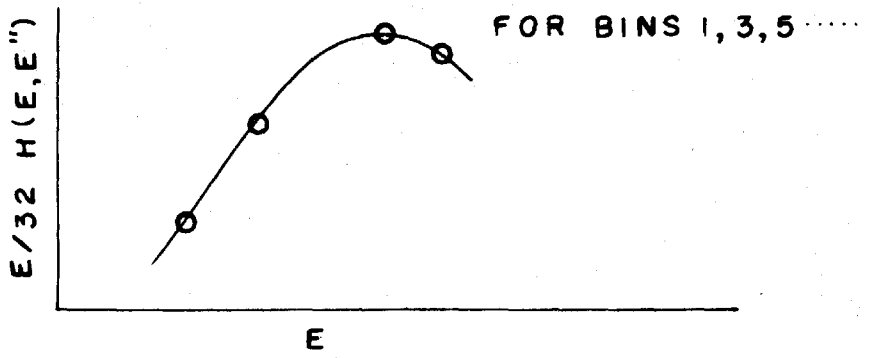

(a)

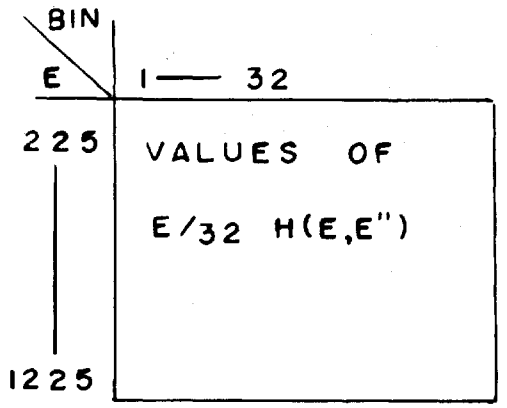

(b)

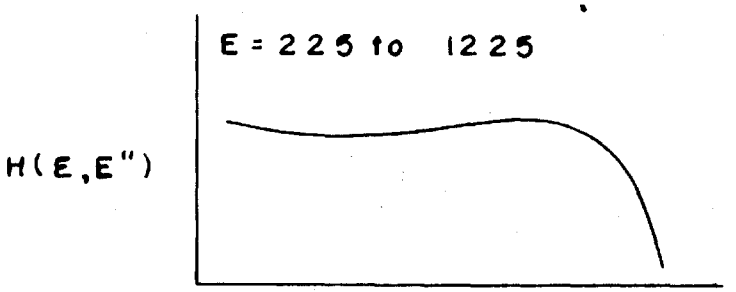

(c)

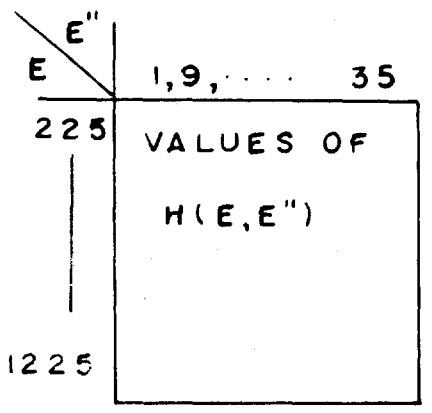

(d)

DIAGRAM 14 (a)(b)(c)(d) - Steps in Matrix Formulation

were read off, and a second table was constructed of E vs E'' with the body containing values of $H(E,E'')$.

The change from intervals in E'' to intervals in Z must be accompanied by a multiplication by 2Z since $Z^2 = E''$, $2ZdZ = dE''$, i.e. $H(y,z) = 2zH(E,E'')$.

Since the bin width in this table is two units of Z wide, the values at the centre of each interval must be multiplied by 2. Thus the body of diagram 14(d) must be multiplied by 4Z to give the non-diagonal elements of the forward matrix M which is presented in Table 3.

The sum of any row in this matrix, corresponding to a particular value of E or y, may be considered as the fraction of photons with energy E which would appear as degraded pulses due to crystal distortions. One would therefore expect the photo peak of the spectrum to contain a fraction $\left\{1 - \Sigma 2H(y,z)\right\}$. This value would appear on the diagonal of the matrix. However, since the photons have a finite probability of passing through the crystal without interacting, the crystal efficiency Y(E) must be taken into account. The total area under the response function R(E,E'') is equal to Y(E). Now $Y(E) = (1 - e^{-\mu L})$ where L is the crystal length, and μ is the linear attenuation coefficient in NaI for photons with energy E. Thus the true function is the peak, i.e. the true diagonal value is

$$\left\{Y(E) - \Sigma 2H(y,z)\right\}$$

Berger & Doggett give crystal efficiencies, for crystals of various sizes, at energies of .279, .661, 1.17, and 1.33 Mev. These values of Y(E) were used to construct a smooth curve, from which the efficiencies at the desired values of E were taken. The diagonal values were then evaluated.

TABLE 3

$y = E^{1/2}$

$z = E''^{1/2}$

FORWARD MATRIX M

(values x 10^3)

y \ z	1	3	5	7	9	11	13	15	17	19	21	23	25	27	29	31	33	35
1	1000																	
3	0	1000																
5	10	30	960															
7	18	54	85	843														
9	0	0	8	59	933													
11	0	0	4	3	25	968												
13	0	0	0	7	8	10	975											
15	1	2	2	2	11	7	6	961										
17	3	9	12	15	15	20	9	0	857									
19	3	9	14	16	19	20	33	11	0	764								
21	3	9	14	18	22	26	28	37	18	0	663							
23	3	9	15	21	26	32	35	41	45	30	0	544						
25	3	10	15	19	24	30	36	43	50	56	40	0	434					
27	3	9	15	20	24	29	37	43	50	52	71	51	3	324				
29	3	8	13	17	22	26	33	39	44	49	49	77	55	5	260			
31	2	6	10	14	18	22	26	32	36	39	42	46	72	54	9	241		
33	2	5	8	12	15	18	21	25	29	32	35	38	49	67	57	9	229	
35	1	4	7	9	12	14	17	19	21	24	27	31	33	50	60	58	13	219

Since the lowest energy considered in the original data of Berger & Doggett was 279 Kev, the response functions were only extrapolated to E = 225 Kev. To fill in the matrix at lower energies, a matrix constructed by Rawson & Cormack (Ref. 9) was used. This matrix could handle energies up to 400 Kev, so there existed a considerable region of overlap. This overlap provided a check on the present matrix, and in fact a smooth transition from one matrix to the other was obtained. The final forward matrix M is shown in Table 3. The matrix M was inverted by the L.G.P. 30 computer through a standard programme, and the inverse matrix M^{-1} is shown in Table 4.

This inverse matrix was used in the correction of measured spectra as follows: the ordinates in a given spectrum N(E'') at values of E'' = 1, 9, 25, ... Kev were read from the graph, converted to N(z) (see Table 2), and arranged as a column vector. The last component of this column consisted of the area of the peak. All the components of the column were then multiplied by their corresponding components in each of the matrix columns, and were added vertically, to give a row of numbers for various values of y = E. This comprised the corrected spectrum N(y) from which the incident photon spectrum N(E) may be obtained (see Table 2). In order to test matrix M^{-1}, a Cs^{137} spectrum was measured and corrected. A small Cs^{137} calibration source (Amersham Model CDCM2, 2 millicuries) was placed in the end of the detector collimator, and its spectrum was measured. This Cs^{137} spectrum was corrected with the matrix, and the latter was found to remove most of the tail, and yield the known Cs^{137} spectrum (diagram 15), that is, a single γ-ray with energy 661 Kev. The inverse matrix was therefore considered to be effective in correcting spectra up to this photon energy.

TABLE 4

$Z = E''^{1/2}$

$y = E^{1/2}$

INVERSE MATRIX M^{-1}

(values x 10^3)

Z \ y	1	3	5	7	9	11	13	15	17	19	21	23	25	27	29	31	33	35
1	1000																	
3	0	1000																
5	-10	-31	1042															
7	-20	-61	-105	1186														
9	1	4	-2	-75	1072													
11	0	0	-4	-2	-28	1033												
13	0	0	0	-8	-8	-11	1026											
15	0	-2	-2	-1	-12	-7	-6	1040										
17	-3	-9	-13	-19	-18	-24	-11	0	1167									
19	-3	-10	-17	-23	-25	-26	-44	-15	0	1309								
21	-4	-11	-18	-29	-33	-39	-43	-58	-32	0	1508							
23	-4	-12	-22	-39	-45	-56	-62	-78	-96	-72	0	1838						
25	-4	-16	-26	-39	-47	-60	-74	-96	-131	-169	-139	0	2304					
27	-5	-15	-29	-47	-53	-64	-88	-110	-157	-198	-329	-289	-21	3086				
29	-6	-13	-23	-36	-47	-54	-75	-97	-132	-186	-248	-539	-487	-59	3846			
31	-2	-4	-9	-20	-26	-32	-37	-54	-71	-96	-138	-266	-665	-689	-144	4149		
33	-1	0	0	-8	-9	-11	-7	-11	-17	-27	-37	-76	-339	-861	-952	-163	4367	
35	-2	0	-1	+1	-1	+1	+3	+11	+17	+15	+17	+28	-12	-455	-959	-109	-259	4560

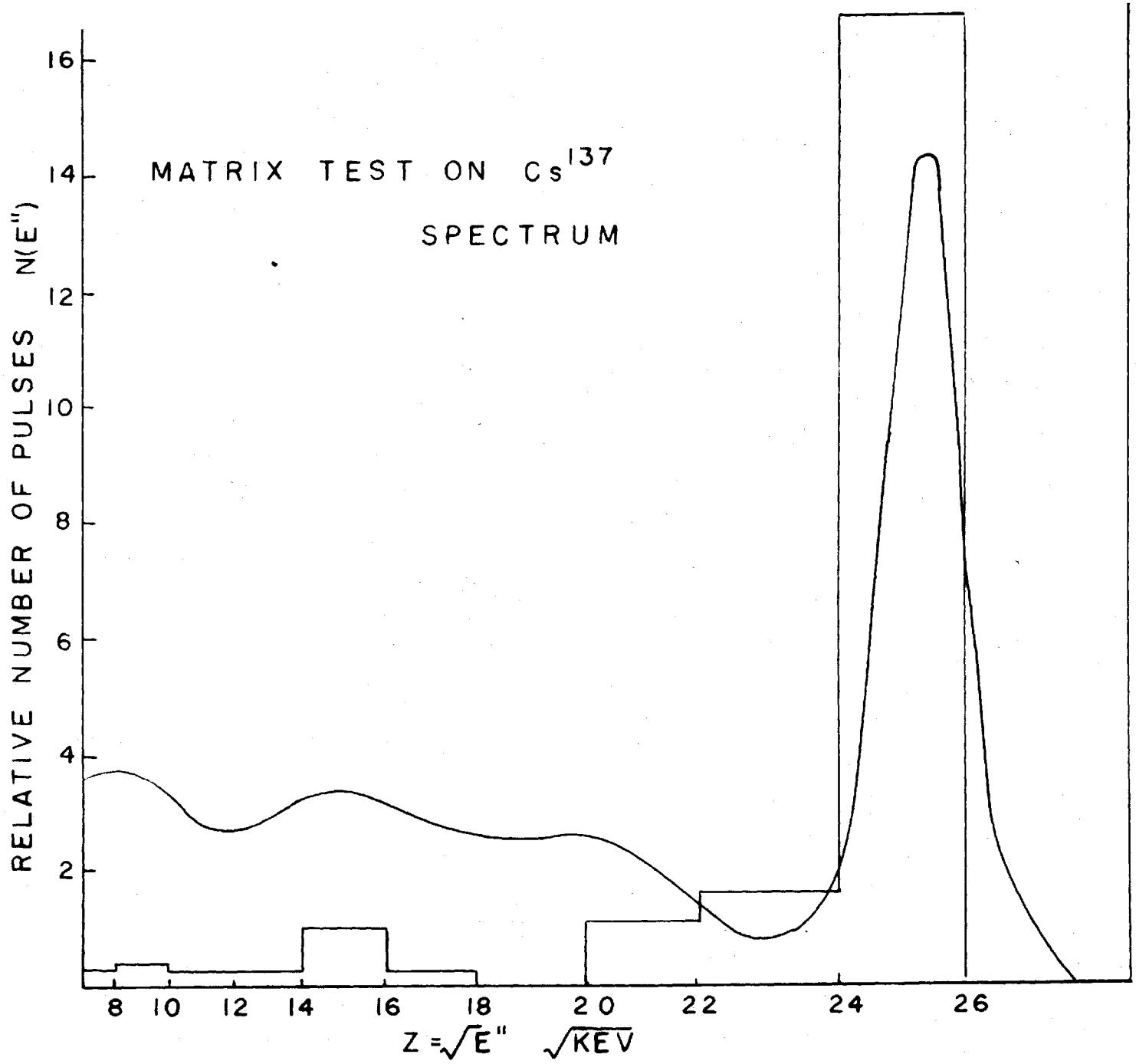

DIAGRAM 15 - Matrix Test on Cs^{137} Spectrum

BIBLIOGRAPHY

1. Cormack, D.V., Till, J.E., Whitmore, G.F. and Johns, H.E.	1955	BJR, 28, 605.
2. Ehrlich, M.	1955	J. Res. N.B.S., 54, 107.
3. Liden, K. and Starfelt, N.	1959	Arkiv Fysik, 7, 427.
4. Skarsgard, L.D. and Johns, H.E.	1961	Rad. Res., 14, 231.
5. Johns, H.E. and MacKay, J.A.	1954	J. Fac. Radiol., 4, 239.
6. Cormack, D.V. and Johns, H.E.	1958	B.J.R., 31, 497.
7. Berger, M.J. and Doggett, J.	1956	J. Res. N.B.S., 56, 355.
8. Hubble, J.H.	1958	Rev. Sci. Inst., 29, 65.
9. Rawson, E.G. and Cormack, D.V.	1958	Nucleonics, 16, 92.